Spin and valley-orbit splittings in SiGe/Si heterostructures

M. O. Nestoklon, L. E. Golub, and E. L. Ivchenko
A.F. Ioffe Physico-Technical Institute, Russian Academy of Sciences, St. Petersburg 194021, Russia
(Received 26 January 2006; published 19 June 2006)

Spin and valley-orbit splittings are calculated in symmetric SiGe/Si/SiGe quantum wells (QWs) by using the tight-binding approach. In accordance with the symmetry considerations an existence of spin splitting of electronic states in perfect QWs with an odd number of Si atomic planes is microscopically demonstrated. The spin splitting oscillates with QW width and these oscillations related to the intervalley reflection of an electron wave from the interfaces. It is shown that the splittings under study can efficiently be described by an extended envelope-function approach taking into account the spin- and valley-dependent interface mixing. The obtained results provide a theoretical base to the experimentally observed electron spin relaxation times in SiGe/Si/SiGe QWs.

DOI: 10.1103/PhysRevB.73.235334 PACS number(s): 73.21.Fg, 72.25.Dc

I. INTRODUCTION

At present various semiconductor materials are being involved in spintronics activities. SiGe/Si quantum well (QW) structures are among them. Silicon-based systems can be particularly promising due to a comparatively weak spin-orbit interaction and long electron spin-relaxation times. Although bulk Si and Ge have an inversion center, QW structures grown from these materials can lack such a center and allow the spin splitting of the electronic subbands, even in the absence of structure inversion asymmetry.[1] An ideal SiGe/Si/SiGe QW structure with an odd number of Si atomic planes is characterized by the D_{2d} point-group symmetry and, therefore, allows spin-dependent linear-in-**k** terms in the electron effective Hamiltonian

$$\mathcal{H}^{(1)}(\mathbf{k}_\parallel) = \alpha(\sigma_x k_x - \sigma_y k_y), \tag{1}$$

where σ_x, σ_y are the spin Pauli matrices, $\mathbf{k}_\parallel$ is the two-dimensional wave vector with the in-plane components k_x, k_y, and $x \| [100], y \| [010]$.

In the present work we use both the microscopic tight-binding model and the envelope-function approach to calculate the spin splitting of the conduction subbands in diamond-lattice QWs. The obtained results are of particular interest in connection with the experimental studies of electron spin relaxation in Si/SiGe heterostructures.[2,3] The consideration of a Si/SiGe structure with perfect interfaces and without built-in electric fields allows one to put the upper limit to the electron spin-relaxation time.

In a bulk homogeneous sample of Si, two of six equivalent minima of the conduction band Δ_1 are located in two points, $\mathbf{k}_0$ and $-\mathbf{k}_0$, along the direction [001] of the first Brillouin zone as illustrated in Fig. 1. The point-group symmetry of a Si/SiGe(001) QW reduces[1] and allows mixing between four bulk Bloch states attached to the $\mathbf{k}_0$ and $-\mathbf{k}_0$ valleys.[4–6] The valley-orbit mixing occurs under electron reflection from a heterointerface: an electron with the wave vector $\mathbf{k}_1 \approx \mathbf{k}_0$ is reflected not only to the state $\mathbf{k}_2$ attached to the same valley $\mathbf{k}_0$ but also to the state $\mathbf{k}_2'$ in the second valley $-\mathbf{k}_0$, see Fig. 1. The reflected wave is a superposition of two waves with their phase difference dependent on the distance z from the interface as $2k_0 z$. In the QW grown along the [001] direction, quantum-confined electron states are standing waves formed as a result of multiple reflection of the four waves $\mathbf{k}_1$, $\mathbf{k}_2$, $\mathbf{k}_1$, $\mathbf{k}_2'$, or $\pm\mathbf{k}_0 \pm (\mathbf{k}_1 - \mathbf{k}_0)$, from the both heterointerfaces.

The spin splitting in conduction subbands is directly related to spin dependence of the electron oblique-incidence reflection from an interface. Spin-dependent reflection of an electron wave from interface consists of intra- and intervalley contributions. The latter should oscillate with the QW width L in the same way as the spin-independent valley-orbit splitting. Thus, interface-induced spin splitting Δ_{spin} contains two contributions: one oscillating with L and another being smooth. Their relation can be obtained in microscopic evaluations.

The paper is organized as follows. In Sec. II we extend the envelope function method to take into account intra- and inter-valley spin-dependent contributions to the effective interface potential. In Sec. III we develop the sp^3s^* tight-binding model in order to calculate the dependence of the coefficient α in Eq. (1) on the QW width, discuss the results of calculations and compare them with the analytical equations derived in Sec. II. The paper is concluded by Sec. IV.

II. EXTENDED ENVELOPE FUNCTION METHOD

Let us consider a QW layer A sandwiched between barriers B and C on the right- and left-hand sides, respectively.

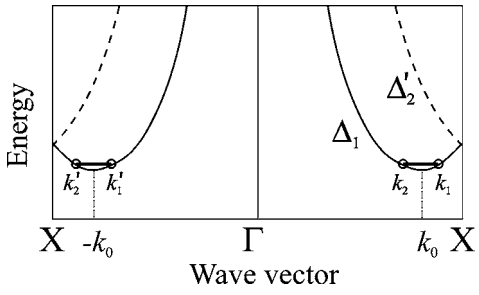

FIG. 1. Schematic representation of the lower conduction bands Δ_1 (solid curve) and Δ_2' (dashed) in bulk Si along the $\Gamma - X$ direction in the first Brillouin zone. Horizontal bars in figure illustrate extension of the $e1$ quantum-confined state in the **k** space; $\mathbf{k}_1$, $\mathbf{k}_2$, $\mathbf{k}_1'$ and $\mathbf{k}_2'$ are wave vectors of four Bloch states mixed in a QW.

We assume that the three bulk materials $j=\mathrm{A},\mathrm{B},\mathrm{C}$ have the diamond-like lattice, the structure is grown along the principal crystallographic axis $z\|[001]$, and the lowest conduction subband $e1$ is formed by electronic states in the two Δ valleys with the extremum points $\pm\mathbf{k}_{0j}=(0,0,\pm k_{0j})$. Note that, in the $Si_{1-x}Ge_x$ solid solution, the extremum-point position is a function of the content x and values of k_{0j} are layer dependent. Because of the lattice constant mismatch some of the structure layers are strained. The layers B and C are assumed to be thick enough for the tunneling tails of the quantum-confined $e1$ states to decay within these layers so that they can be considered as semi-infinite.

In the generalized envelope function approximation the electron wave function $\Psi(\mathbf{r})$ inside the layer j is written as

$$\Psi(\mathbf{r}) = e^{i\mathbf{k}_\parallel\cdot\boldsymbol{\rho}}[\varphi_1(z;j)\psi_{\mathbf{k}_{0j}}(\mathbf{r}) + \varphi_2(z;j)\psi_{-\mathbf{k}_{0j}}(\mathbf{r})]. \quad (2)$$

Here

$$\psi_{\mathbf{k}_{0j}}(\mathbf{r}) = e^{ik_{0j}z}u_{\mathbf{k}_{0j}}(\mathbf{r}),$$

$$\psi_{-\mathbf{k}_{0j}}(\mathbf{r}) = e^{-ik_{0j}z}u_{-\mathbf{k}_{0j}}(\mathbf{r}) \quad (3)$$

are the scalar Bloch functions at the two Δ extremum points, $u_{\pm\mathbf{k}_{0j}}(\mathbf{r})$ are the Bloch periodic amplitudes, $\varphi_1(z;j)$ and $\varphi_2(z;j)$ are the smooth spinor envelope functions defined within the layer j, $\boldsymbol{\rho}$ is the in-plane component of the three-dimensional radius-vector $\mathbf{r}$.

The two-valley effective Hamiltonian $\mathcal{H}$ is presented as a sum of the zero-order valley- and spin-independent term

$$\mathcal{H}_0 = \frac{\hbar^2}{2}\left[-\frac{d}{dz}\frac{1}{m_l(z)}\frac{d}{dz} + \frac{k_x^2+k_y^2}{m_t(z)}\right] \quad (4)$$

and the interface-induced δ-functional perturbation

$$\mathcal{H}' = V_L\delta(z-z_L) + V_R\delta(z-z_R). \quad (5)$$

Here m_l and m_t are the longitudinal and transverse effective masses for electrons in the Δ valley, z_L and z_R are the coordinates of the left- and right-hand side interfaces, V_L and V_R are both valley- and spin-dependent operators. Hereafter we assume that the latter contain no differentiation d/dz; this assumption excludes the need in symmetrization of $V_{L,R}$ and the δ function.

The form of V_L, V_R can be specified by applying the symmetry considerations. A single (001) interface is characterized by the C_{2v} point-group symmetry allowing two linear-$\mathbf{k}_\parallel$ spin-dependent invariants, namely

$$h(\mathbf{k}) = \sigma_x k_x - \sigma_y k_y \quad \text{and } h'(\mathbf{k}) = \sigma_x k_y - \sigma_y k_x.$$

It follows then that the matrices V_m $(m=L,R)$ acting on the bispinor vector with components $\varphi_{1,1/2}, \varphi_{1,-1/2}, \varphi_{2,1/2}, \varphi_{2,-1/2}$ can be presented in the form of a 2×2 block matrix

$$V_m = \begin{bmatrix} S_m h(\mathbf{k}) + S'_m h'(\mathbf{k}) & \Lambda_m I + P_m h(\mathbf{k}) + P'_m h'(\mathbf{k}) \\ \Lambda_m^* I + P_m^* h(\mathbf{k}) + P_m'^* h'(\mathbf{k}) & S_m h(\mathbf{k}) + S'_m h'(\mathbf{k}) \end{bmatrix} \quad (6)$$

with its components being linear combinations of the Pauli matrices and the 2×2 unit matrix I. Here $\mathbf{k}\equiv\mathbf{k}_\parallel$, and $S_m, S'_m, \Lambda_m, P_m, P'_m$ are coefficients characterizing the right-hand $(m=R)$ and left-hand $(m=L)$ interfaces; the first two of them (S_m, S'_m) are real while others are complex. The diagonal components $V_{m;11}=V_{m;22}$ give intra-valley contributions, whereas the off-diagonal components $V_{m;12}=V_{m;21}^\dagger$ describe interface-induced inter-valley mixing. It is more convenient to perform the further considerations for a particular case of coinciding barriers, C=B, and coinciding extremum points, $\mathbf{k}_{0\mathrm{B}}=\mathbf{k}_{0\mathrm{A}}$. Then we briefly discuss how these considerations are generalized with allowance for C≠B and different positions of extremum points $\mathbf{k}_{0j}$.

The choice of the electron Hamiltonian in the form of Eqs. (4) and (5), corresponds to a particular set of boundary conditions. For the structure B/A/B with $k_{0\mathrm{B}}=k_{0\mathrm{A}}\equiv k_0$, this set reads

$$\varphi(z_L+0) = \varphi(z_L-0), \quad \varphi(z_R+0) = \varphi(z_R-0),$$

$$\frac{1}{m_l(\mathrm{B})}\left(\frac{d\varphi}{dz}\right)_{z_L-0} = \frac{1}{m_l(\mathrm{A})}\left(\frac{d\varphi}{dz}\right)_{z_L+0} + \frac{2}{\hbar^2}V_L\varphi(z_L),$$

$$\frac{1}{m_l(\mathrm{B})}\left(\frac{d\varphi}{dz}\right)_{z_R+0} = \frac{1}{m_l(\mathrm{A})}\left(\frac{d\varphi}{dz}\right)_{z_R-0} - \frac{2}{\hbar^2}V_R\varphi(z_R), \quad (7)$$

where $\varphi(z_{L,R}\pm 0)$, $(d\varphi/dz)_{z_{L,R}\pm 0}$ are the envelope function and its first derivative at z approaching the interface L,R from the right- (+0) and left-hand (−0) sides.

The next step is to analyze the phases of the coefficients Λ_m, P_m, P'_m in the off-diagonal components of V_m and establish a relation between V_L and V_R. First of all, we take into account that the translation of the radius-vector $\mathbf{r}$ by a three-dimensional Bravais-lattice vector $\mathbf{a}$ results in a multiplication of the Bloch functions $\psi_{\pm\mathbf{k}_{0j}}(\mathbf{r})$ in Eq. (3) by the factors $\exp(\pm ik_{0j}a_z)$, respectively. Therefore, one can present the coefficients in the off-diagonal components of V_m as[7,8]

$$\Lambda_m = \lambda_m e^{-2ik_{0z}z_m},$$

$$P_m = p_m e^{-2ik_{0z}z_m}, \quad P'_m = p'_m e^{-2ik_{0z}z_m}, \quad (8)$$

where the complex coefficients λ_m, p_m, p'_m are independent of the interface position. In the following we assume the origin $z=0$ to lie in the QW center.

The structure B/A/B is invariant under the mirror rotation operation $\mathcal{S}_4$ with the transformation center at $z=0$, if the number N of atomic planes in the layer A is odd, and under the space inversion operation i, if N is even.[1] This symmetry property allows one to establish the relations between the coefficients in Eq. (6) for the left- and right-hand side interfaces. Since both operations result in the reciprocal transformation $\psi_{\mathbf{k}_{0j}}(\mathbf{r}) \leftrightarrow \psi_{-\mathbf{k}_{0j}}(\mathbf{r})$ one has

$$\begin{bmatrix} 0 & \lambda_\mathrm{L} \\ \lambda_\mathrm{L}^* & 0 \end{bmatrix} = \begin{bmatrix} 0 & 1 \\ 1 & 0 \end{bmatrix}\begin{bmatrix} 0 & \lambda_\mathrm{R} \\ \lambda_\mathrm{R}^* & 0 \end{bmatrix}\begin{bmatrix} 0 & 1 \\ 1 & 0 \end{bmatrix}$$

or, equivalently, $\lambda_\mathrm{L}=\lambda_\mathrm{R}^*$. Taking into account that, under the mirror-rotation operation $\mathcal{S}_4$, the C_{2v}-group invariants $h(\mathbf{k})$ and $h'(\mathbf{k})$ transform, respectively, into $h(\mathbf{k})$ and $-h'(\mathbf{k})$ while, under the space inversion i, both $h(\mathbf{k})$ and $h'(\mathbf{k})$ change their sign, we also obtain the relations

$$S_R = S_L, \quad S'_R = -S'_L, \quad p_R = p^*_L, \quad p'_R = -p'^*_L \tag{9}$$

for odd N and

$$S_R = -S_L, \quad S'_R = -S'_L, \quad p_R = -p^*_L, \quad p'_R = -p'^*_L \tag{10}$$

for even N. Hereafter we use the notations λ, S, S', p, p' instead of $\lambda_R, S_R, S'_R, p_R, p'_R$. By using Eqs. (9) and (10) we can reduce the components in the matrix (6) to

$$V_{R,11} = V_{R,22} = Sh(\mathbf{k}) + S'h'(\mathbf{k}), \tag{11}$$

$$V_{L,11} = V_{L,22} = Sh(\mathbf{k}) - S'h'(\mathbf{k}),$$

$$V_{R,12} = V^*_{R,21} = e^{-ik_0L}[\lambda I + ph(\mathbf{k}) + p'h'(\mathbf{k})],$$

$$V_{L,12} = V^*_{L,21} = e^{ik_0L}[\lambda^* I + p^* h(\mathbf{k}) - p'^* h'(\mathbf{k})]$$

if N is odd, and to

$$V_{R,11} = V_{R,22} = Sh(\mathbf{k}) + S'h'(\mathbf{k}),$$

$$V_{L,11} = V_{L,22} = -Sh(\mathbf{k}) - S'h'(\mathbf{k}),$$

$$V_{R,12} = V^*_{R,21} = e^{-ik_0L}[\lambda I + ph(\mathbf{k}) + p'h'(\mathbf{k})],$$

$$V_{L,12} = V^*_{L,21} = e^{ik_0L}[\lambda^* I - p^* h(\mathbf{k}) - p'^* h'(\mathbf{k})] \tag{12}$$

if N is even. Here $L = z_R - z_L$ is the QW width, it is given by $L = Na_0/4$ with a_0 being the zinc blende lattice constant.

Equations (11) and (12) present the results of the extended envelope-function method and yield relations between coefficients in the matrices V_L and V_R for macroscopically symmetric QWs.

If the barriers are grown from different materials B and C then the coefficients in Eqs. (11) and (12) should be labeled by the interface index, C/A or B/A, e.g., $S(\mathrm{C/A})$ and $p'(\mathrm{B/A})$. The different positions of the extremum points $\mathbf{k}_{0j}$ are easily taken into account by replacing $\varphi_1(z;j)$ and $\varphi_2(z;j)$ $(j = \mathrm{B}, \mathrm{C})$ in Eq. (2) and in the boundary conditions (7) by

$$\tilde{\varphi}_1(z;j) = e^{i(\mathbf{k}_{0j} - \mathbf{k}_{0A})z_j}\varphi_1(z;j),$$

$$\tilde{\varphi}_2(z;j) = e^{-i(k_{0j} - k_{0A})z_j}\varphi_2(z;j),$$

where z_j is the coordinate of the interface between the layers A and $j = \mathrm{C}$ or B. This replacement allows to retain the form of the perturbation $\mathcal{H}'$ defined by Eqs. (5), (6), and (8).

A. Valley-orbit splitting

The numerical calculations presented in the following sections confirm the hierarchy

$$E_X - E(\mathbf{k}_0) \gg E_{e1} \gg \Delta_{v\text{-}o} \gg \Delta_{spin} \equiv \alpha_\pm k \tag{13}$$

illustrated by Fig. 2(a). Here $E(\mathbf{k}_0)$ and E_X are the conduction-band energies at the extremum point $\mathbf{k}_0$ and the X point in the bulk material A, E_{e1} is the quantum-confinement energy for the lowest conduction subband, $\Delta_{v\text{-}o}$ and Δ_{spin} are the valley-orbit and spin splitting of the $e1$-subband states.

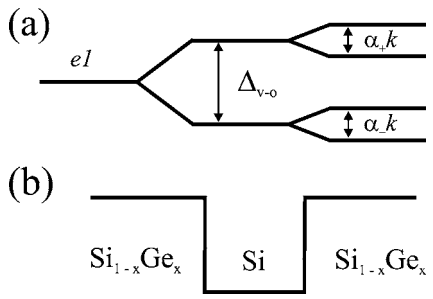

FIG. 2. Schematic representation of (a) hierarchy of the $e1$ subband splittings and (b) the $Si/Si_{1-x}Ge_x$ structure under consideration. We remind that, in this structure, the conduction band offset is mostly determined by the strain.

Therefore, we can line up the discussion in series starting from the quantum confinement, turning then to the valley-orbit splitting and finally to the spin splitting. As above we start from the analysis of the symmetric structure B/A/B shown schematically in Fig. 2(b) and then generalize the results on asymmetric structures with different barriers B and C.

For eigenstates of the zero-approximation Hamiltonian $\mathcal{H}_0$ the inter-valley mixing is absent and the envelope functions referred to the first and second (001)-valleys form identical sets. In particular, for the $e1$ subband states in the B/A/B structure, the envelope has the standard form

$$\chi(z) = c\begin{cases} \cos qz, & |z| \leqslant L/2 \\ \cos(qL/2)\exp[-æ(|z| - L/2)], & |z| \geqslant L/2 \end{cases}. \tag{14}$$

Here $q = [2m_l(\mathrm{A})E_{e1}/\hbar^2]^{1/2}$, $æ = [2m_l(\mathrm{B})(V - E_{e1})/\hbar^2]^{1/2}$ and c is the normalization factor. The size-quantization energy E_{e1} satisfies the transcendental equation $\tan(qL/2) = (æ/q) \times [m_l(\mathrm{A})/m_l(\mathrm{B})]$.

Now we switch on the inter-valley mixing taking into account zero-$\mathbf{k}$ terms in Eqs. (11) and (12) proportional to λ and λ^*. According to Eqs. (5), (11), and (12) the matrix element of the inter-valley coupling is given by

$$M_{1,s;2,s'} = |\chi(L/2)|^2(V_{R,12} + V_{L,12}) = 2|\chi(L/2)|^2|\lambda|\cos(k_0L - \phi_\lambda)\delta_{ss'}, \tag{15}$$

where $|\lambda|$ and ϕ_λ are the modulus and the phase of λ, and s, $s' = \pm 1/2$ are the electron spin indices. Thus, the energies of the split $e1$ states at $k_x = k_y = 0$ are

$$E_{e1,\pm} = \pm 2|\chi(L/2)|^2 \cdot |\lambda \cos(k_0L - \phi_\lambda)| \tag{16}$$

and the envelopes are

$$\varphi_1(z; e1, \pm) = \pm \eta\varphi_2(z; e1, \pm) = \chi(z)/\sqrt{2}, \tag{17}$$

where $\chi(z)$ is defined in Eq. (14) and $\eta = \mathrm{sign}\{\cos(k_0L - \phi_\lambda)\}$. Therefore, the parity of the lower state $|e1, -\rangle$ (with respect to the operation $\mathcal{S}_4$ if N is odd and i if N is even) follows the sign of η and reverses with the reversal of η.

Equation (16) expresses an oscillating character of $\Delta_{\text{v-o}}(L)$ in terms of the envelope function method. It will be shown in Sec. III that this agrees with the tight-binding numerical results.

For an asymmetric C/A/B structure, the inter-valley matrix element and $e1$-subband energies are generalized to

$$M_{1,s;2,s'} = |\chi(L/2)|^2(\lambda_R e^{-ik_{0A}L} + \lambda_L e^{ik_{0A}L})\delta_{ss'},$$

$$E_{e1,\pm} = \pm|\chi(L/2)|^2[|\lambda_R|^2 + |\lambda_L|^2 + 2|\lambda_R\lambda_L|\cos(2k_{0A}L + \phi_{\lambda_L} - \phi_{\lambda_R})]^{1/2}, \quad (18)$$

where ϕ_{λ_m} is the phase of λ_m $(m=\text{R},\text{L})$.

B. Spin-orbit splitting

The next step is to take into account spin-dependent terms in V_m. Since the symmetry forbids spin-splitting of the electron states in the B/A/B system with an even number of atomic planes in the A layer, we set N to be odd. Then the inter-valley mixing is described by the matrix elements

$$M_{1,s;2,s'} = 2|\chi(L/2)|^2[|\lambda|\cos(k_0L - \phi_\lambda)\delta_{ss'} + |p|\cos(k_0L - \phi_p)h_{ss'}(\mathbf{k}) - i|p'|\sin(k_0L - \phi_{p'})h'_{ss'}(\mathbf{k})], \quad (19)$$

where ϕ_p, $\phi_{p'}$ are the phases of p and p'. Assuming the valley-orbit splitting to exceed the spin-orbit splitting we are able to rewrite the Hamiltonian in the basis (17) and obtain the following 2×2 spin-dependent effective Hamiltonians in the subbands $(e1,\pm)$

$$\mathcal{H}'(\mathbf{k};e1,\pm) = |\chi(L/2)|^2[V_{\text{L},11} + V_{\text{R},11} \pm \eta\,\text{Re}(V_{\text{L},12} + V_{\text{R},12})], \quad (20)$$

and finally

$$\mathcal{H}(\mathbf{k};e1,\pm) = E_{e1,\pm} + \alpha_\pm h(\mathbf{k}), \quad (21)$$

where the coefficients in the linear-$\mathbf{k}$ term are given by

$$\alpha_\pm = 2|\chi(L/2)|^2[S \pm |p|\,\eta\cos(k_0L - \phi_p)]. \quad (22)$$

While deriving Eq. (22) we took into account both the intra- and inter-valley contributions to V_m and retained only the terms up to the first order in S and p. In agreement with the symmetry arguments, neither the S'-dependent nor p'-dependent contributions to V_m give rise to linear-$\mathbf{k}$ terms. Note that, for the sake of completeness, in addition to the linear-$\mathbf{k}$ terms one can include in the right-hand side of Eq. (22) a spin-independent quadratic-$\mathbf{k}$ term $\hbar^2\mathbf{k}^2/2m_\parallel$. Here $m_\parallel^{-1} = \langle e1|m_\parallel^{-1}(z)|e1\rangle$ and the angle brackets mean averaging over the $e1$ state defined in Eq. (14).

In addition to a smoothly decreasing term in $\alpha_\pm$ predicted in Ref. 1, Eq. (22) contains an oscillating term. The reason for the oscillations is mixing of valley states at the QW interfaces. Tight-binding calculations presented below show that $|p| > S$, i.e., the oscillating part of $\alpha_\pm$ is dominating.

For an asymmetric structure C/A/B, the linear-$\mathbf{k}$ contribution to the Hamiltonian $\mathcal{H}(\mathbf{k};e1,\pm)$ takes the form

$$\mathcal{H}^{(1)}(\mathbf{k};e1,\pm) = \alpha_\pm h(\mathbf{k}) + \beta_\pm h'(\mathbf{k})$$

with

$$\alpha_\pm = |\chi(L/2)|^2[S_R + S_L \pm \text{Re}\{e^{-i\xi}(p_R e^{-ik_0L} + p_L e^{ik_0L})\}],$$

$$\beta_\pm = |\chi(L/2)|^2[S'_R + S'_L \pm \text{Re}\{e^{-i\xi}(p'_R e^{-ik_0L} + p'_L e^{ik_0L})\}], \quad (23)$$

and $\xi = \arg\{\lambda_R e^{-ik_0L} + \lambda_L e^{ik_0L}\}$. For the symmetric structure, $e^{i\xi} = \eta = \pm 1$.

III. TIGHT-BINDING CALCULATIONS AND DISCUSSION

In order to estimate values of spin and valley-orbit splittings we have performed calculations of the electron dispersion in the $e1$ conduction subband by using one of the empirical tight-binding models. More precisely, we have fixed on the nearest-neighbor sp^3s^* tight-binding model optimized for the conduction band.[9] This model is a reasonable compromise between the numerical load and the accuracy of representation of the band structure. It is capable of reproducing the indirect gap although it shifts the position of the conduction band minimum from the experimentally measured point $k_0 = 0.85\times2\pi/a_0$ to the point $k_0 = 0.62\times2\pi/a_0$. Note that a value of k_0 is hardly reproduced even in the more sophisticated methods, namely, the second-nearest neighbor sp^3s^* and nearest-neighbor $sp^3d^5s^*$ tight-binding models,[10,11] leading to $k_0a_0/2\pi = 0.758$ and 0.813, respectively. The applicability of the sp^3s^* model is confirmed by the fact, see below, that values of the valley-orbit splitting $\Delta_{\text{v-o}}$ calculated in this work and by using the $sp^3d^5s^*$ model[5] are of the same order of magnitude.

The empirical sp^3s^* tight-binding method was previously applied for calculation of the spin splitting in bulk GaAs and GaAs-based QWs.[12] The linear-in-$\mathbf{k}$ splitting in a QW was compared with the cubic spin splitting in bulk GaAs where the component k_z was replaced by π/d_{GaAs} with d_{GaAs} being the width of the GaAs layer. The agreement was obtained after replacing d_{GaAs} by an effective value $d^{\text{eff}}_{\text{GaAs}}$ and adjusting the coefficient γ in the cubic-in-$\mathbf{k}$ contribution to the electron effective Hamiltonian $\mathcal{H}^{(1)}(\mathbf{k})$. The need in the introduction of the effective parameters $d^{\text{eff}}_{\text{GaAs}}$ and γ^{eff} can be related to an additional contribution to $\mathcal{H}^{(1)}(\mathbf{k})$ coming from the reduced symmetry of interfaces, or, in other words, from the anisotropic orientation of interface bonds.[13] In contrast to the zinc blende lattice heterostructures, in diamond-lattice QWs the Hamiltonian $\mathcal{H}^{(1)}(\mathbf{k})$ has no bulk inversion asymmetry term proportional to γ and is contributed only by the interface inversion asymmetry term described by the coefficient α in Eq. (1).[1]

In the tight-binding method the electron Hamiltonian is presented by a set of matrix elements taken between atomic orbitals. If a heterostructure is grown from diamond-like semiconductors along the [001] principal axis one can write the tight-binding free-electron wave function

$$\psi = \sum_{n,\nu} c_{n,\nu}\Phi_{n,\nu,\mathbf{k}}(\mathbf{r}) \quad (24)$$

in terms of planar orbitals

TABLE I. Tight-binding parameters used in the calculations in eV.

	E_s	E_p	E_{s^*}	V_{ss}	V_{xx}	V_{xy}	V_{sp}	V_{s^*p}	Δ
Si	−3.65866	1.67889	3.87576	−7.97142	1.69558	23.32410	8.87467	5.41174	0.045
Ge	−5.88	1.61	6.39	−6.78	1.61	4.90	5.4649	5.2191	0.30

$$\Phi_{n,\nu,\mathbf{k}}(\mathbf{r}) = \sum_m e^{i\mathbf{k}\cdot\mathbf{r}_m}\Phi_\nu(\mathbf{r}-\mathbf{r}_m). \quad (25)$$

Here $n=0,\pm1,\pm2\ldots$ is the number of atomic planes perpendicular to the growth direction $z\|[001]$, Φ_ν is the orthogonalized atomic orbital with ν being the orbital index, the index m enumerates atoms in the nth atomic plane, $\mathbf{r}_m$ is the position of the mth atom in this plane, in particular, $z_m = na_0/4$, $\mathbf{k}$ is the two-dimensional in-plane electron wave vector. The index ν runs through $2N$ values where N is the number of orbitals taken into consideration and the factor is due to electron spin. For convenience we use below the Cartesian coordinate system $x'\|[1\bar{1}0], y'\|[110], z\|[001]$. In the nearest-neighbor approximation we obtain the following set of equations

$$\hat{U}^\dagger_{y'}(2l)C_{2l-1} + \hat{E}_0(2l)C_{2l} + \hat{U}_{x'}(2l)C_{2l+1} = EC_{2l},$$

$$\hat{U}^\dagger_{x'}(2l-1)C_{2l-2} + \hat{E}_0(2l-1)C_{2l-1} + \hat{U}_{y'}(2l-1)C_{2l} = EC_{2l-1} \quad (26)$$

for the vectors C_n containing $2N$ components $c_{n,\nu}$. Here $\hat{E}_0(n)$ is $\mathbf{k}$-independent diagonal matrices, $\hat{U}_{x'}$ and $\hat{U}_{y'}$ are $k_{x'}$ and $k_{y'}$ dependent matrices. The diamond lattice has two atoms per unit cell and can be represented as two face-centered cubic sublattices shifted with respect to each other by $\sqrt{3}a_0/4$ along the [111] direction. The atomic planes with even $n=2l$ and odd $n=2l+1$ ($l=0,\pm1\ldots$) belong to the different sublattices and differ in the direction of chemical bonds. As compared with the pair of planes $2l$ and $2l+1$, the orientation of chemical bonds between atoms in the planes $2l-1$ and $2l$ is rotated around the axis z by 90°. For brevity we omit here the detailed form of matrices $\hat{U}_{x',y'}(n)$; for $k_{x'}=k_{y'}=0$ these matrices can be readily obtained from those for the zinc blende based heterostructures given in Ref. 14. The matrices $\hat{E}_0$, $\hat{U}_{x',y'}$ are formed by the tight-binding parameters, which are usually extracted from fitting bulk-material band structure to experimental one. The tight-binding parameters for Si and Ge are listed in Table I. The diagonal energies are referred to the valence band top of each material. The parameters for Si were taken from Ref. 9; those for Ge are not so critical for the purpose of this work, we collected them from Ref. 15 and added a value of 0.30 eV for the spin-orbit splitting of the p orbitals.[11] For SiGe alloys, we have used the virtual crystal approximation and the linear interpolation of the tight-binding parameters. The strain was taken into account only by shifting the diagonal energies $E_{0,\nu}$ in Si or Ge by the same value, the strain-induced splitting of the p-orbital states was ignored. The shift of diagonal energies for the barrier material is equal to $\Delta E_c - \Delta E_g$, where ΔE_g is the difference in the band gaps of the well and barrier bulk materials and ΔE_c is the conduction-band offset. For a $Si_{1-x}Ge_x/Si/Si_{1-x}Ge_x$ QW structure with the strained Si layer and the Ge content $x=0.25$ we used a value of $\Delta E_c = 0.15$ eV relying on Refs. 2, 5, 16, and 17.

Squares in Fig. 3 show results of tight-binding calculations of the valley-orbit splitting $\Delta_{v\text{-}o}$ in symmetrical $Si_{0.75}Ge_{0.25}/Si/Si_{0.75}Ge_{0.25}$ QWs as a function of the number N of Si atomic planes sandwiched between the thick barriers $Si_{0.75}Ge_{0.25}$. The valley-orbit splitting exhibits pronounced oscillations with the increasing QW width, in agreement with Refs. 4–6. The oscillation periods in Fig. 3 of the present work and in Fig. 3 of Ref. 6 vary considerably due to the difference in values of $\mathbf{k}_0$ obtained in the sp^3s^* model used here and the $sp^3d^5s^*$ model. However, the splittings $\Delta_{v\text{-}o}$ are of the same order of magnitude, e.g., at $N\approx60$ the oscillation amplitudes differ only by a factor of ~2 which can be explained by the obvious sensitivity of $\Delta_{v\text{-}o}$ to the model used.

Crosses in Fig. 3 represent the calculation of $\Delta_{v\text{-}o}$ in the envelope-function approximation, Eq. (16), with $k_0=0.62\times2\pi/a_0$. While calculating the electron envelope function at the interface, $\chi(L/2)$, we used values of $V=150$ meV for the conduction-band offset and of $0.907m_0$ (m_0 is the free electron mass) for the longitudinal effective mass m_l(A) as obtained in the sp^3s^* tight-binding model optimized for the conduction band,[9] and, for simplicity, took m_l(B) equal to m_l(A). The modulus $|\lambda|$ and the phase ϕ_λ were considered in Eq. (16) as adjustable parameters. Their best fit values turned out to be $|\lambda|=385$ meV·Å, $\phi_\lambda=0.3\pi$. It is seen from Fig. 3

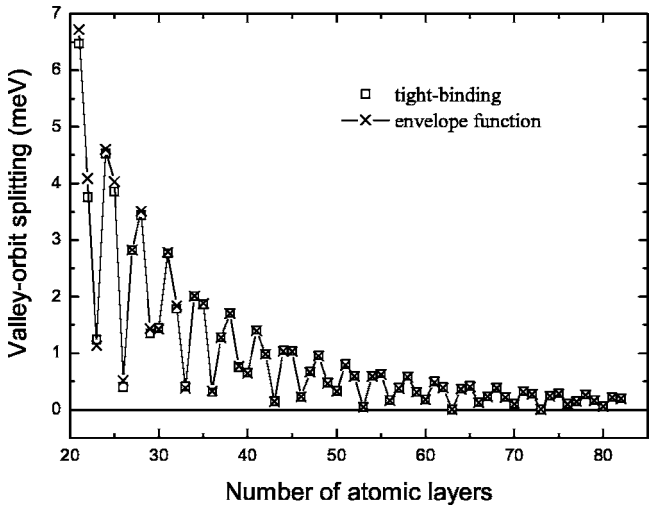

FIG. 3. Valley-orbit splitting $\Delta_{v\text{-}o}$ in $Si_{1-x}Ge_x/Si/Si_{1-x}Ge_x$ ($x=0.25$) QW versus the number of Si mono atomic layers. Analytical results shown by crosses calculated using Eq. (16) with $|\lambda|=385$ meV·Å, $\phi_\lambda=0.3\pi$.

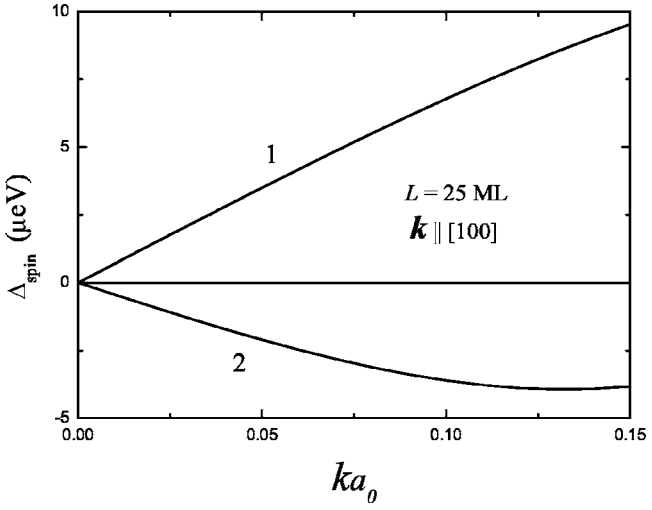

FIG. 4. Spin splitting of the valley-orbit split subbands in a $Si_{0.75}Ge_{0.25}/(Si)_N Si_{0.75}Ge_{0.25}$ QW with $N=25$ as a function of the in-plane wave vector for $\mathbf{k}\|[100]$. Curves 1 and 2 correspond to the subbands $E_{e1,+}$ and $E_{e1,-}$, respectively. The definition of the sign of Δ_{spin} is given in the text.

that the simple analytical theory developed in Sec. II in complete agreement with the results of more sophisticated tight-binding calculations.

In Figs. 4 and 5 the spin-orbit splitting for the two valley-orbit subbands $E_{e1,-}$ and $E_{e1,+}$ are presented. This is the first calculation of the spin splitting, no previous theoretical estimations are available in order to compare with. We define the splitting Δ_{spin} in Fig. 5 as the energy difference between the states with the spin parallel and antiparallel to the x axis for $k_y=0$. Then if the antiparallel state lies higher the sign of Δ_{spin} is negative as in case of the upper valley-orbit split subband $E_{e1,+}$, see curve 2 in Fig. 4. The calculation shows that, up to $k \leqslant 10^6$ cm^{-1}, the linear dependence

$$\Delta_{\text{spin}}(k) = 2\alpha_{\pm}k \tag{27}$$

holds, in agreement with the Hamiltonian (22). It is the variation of $\alpha_{\pm}$ with odd N which is shown in Fig. 5. As one can see from Figs. 3–5 the valley-orbit and spin splittings are conveniently presented in the meV and μeV scales confirming our assumption (13).

Figure 5 shows that the spin splitting Δ_{spin} is an oscillating function of the QW width. This demonstrates that the inter-valley spin-dependent mixing at the interfaces prevails over the intra-valley contribution to $\alpha_{\pm}$. Squares and diamonds in Fig. 5 show results of tight-binding calculation. The spin splitting is plotted only for odd number of Si monoatomic planes because, for even N, Δ_{spin} in the symmetric structures vanishes. Conventional and $\times$-shaped crosses are obtained as the best fit using Eq. (22) and choosing the same values for k_0 and ϕ_λ as in Fig. 3 and the additional adjustable parameters $|p|=0.53\times10^{-18}$ eV cm^2, $\phi_p=0.17\pi$, $S=0.15|p|$.

Now we compare the value of α_- estimated in this work with that extracted by Wilamowski *et al.*[2] from spin-resonance measurements in a $Si/Si_{1-x}Ge_x$ QW structure with $x=0.25$. Note that the value $\alpha_-=0.55\times10^{-12}$ eV·Å presented in this reference for a 120-Å-thick QW should be decreased by a factor of 1.6, i.e., in fact $\alpha_-=0.34\times10^{-12}$ eV·Å, see Ref. 18. Our estimation of α_- gives a value smaller by a factor ~6. This means that in the sample studied in Ref. 2 the Rashba (or structure-inversion asymmetry[19]) contribution to the spin splitting dominates over the intrinsic contribution considered here. Nevertheless, the experimental value of the spin splitting is not so far from the limit for a perfect QW structure.

It is also worth noting that the interface roughness with monoatomic height steps results in the formation of antiphased domains. In the QW with an odd number of Si atomic planes, within each domain, the local symmetry is still D_{2d}. However, the coefficient α in Eq. (1) has opposite signs in different domains, see Ref. 1 and references therein.

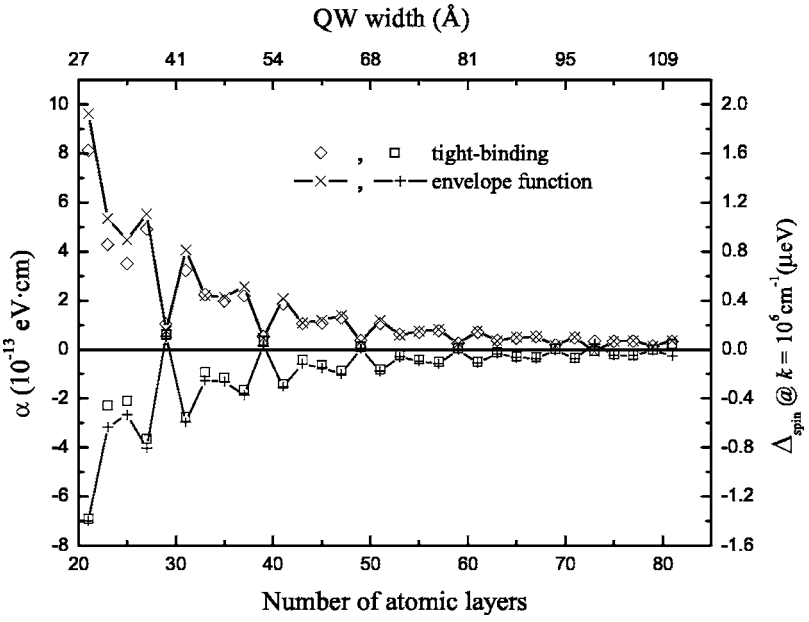

FIG. 5. Spin-splitting constant α in Eqs. (21) and (27) versus the QW width determined by the number of Si monoatomic layers (odd N are taken in consideration only). The spin splitting of the lower subband E_{e1-} is shown by diamonds (tight-binding calculation) and $\times$-shaped crosses (envelope function approximation), those for the upper subband E_{e1+} are shown by squares and conventional crosses.

IV. CONCLUSION

The sp^3s^* tight-binding model has been developed in order to calculate the electron dispersion in heterostructures grown from multivalley semiconductors with the diamond lattice, particularly, in the Si/SiGe structures. The model allows one to estimate the valley-orbit and spin-orbit splittings of the electron quantum-confined states in the ground subband. In the employed tight-binding model, the spin-orbit splitting is mostly determined by the spin-dependent orbit-valley mixing at the interfaces. For this reason the coefficients $\alpha_{\pm}$ describing the linear-in-**k** splitting are strongly oscillating functions of the odd number, N, of the Si monoatomic layers.

In addition to the numerical calculations, an envelope-function approximation has been extended to take account of spin-dependent reflection of an electronic wave at the interface and interface-induced inter-valley mixing. The dependencies of the valley-orbit and spin-orbit splittings upon the number of Si atomic planes calculated in the tight-binding microscopic model are successfully reproduced by using simple analytical equations derived in the envelope-function theory and fitting the parameters that enter into these equations. It follows then that the envelope-function approach can be applied as well for the description of electron-subband splittings in a realistic Si/SiGe structure.

ACKNOWLEDGMENTS

This work was financially supported by the RFBR, programmes of RAS, "Dynasty" Foundation—ICFPM, RSSF, and Russian President grant for young scientists.

[1] L. E. Golub and E. L. Ivchenko, Phys. Rev. B **69**, 115333 (2004).
[2] Z. Wilamowski, W. Jantsch, H. Malissa, and U. Rössler, Phys. Rev. B **66**, 195315 (2002).
[3] A. M. Tyryshkin, S. A. Lyon, W. Jantsch, and F. Schäffler, Phys. Rev. Lett. **94**, 126802 (2005).
[4] F. J. Ohkawa, Solid State Commun. **26**, 69 (1978).
[5] T. B. Boykin, G. Klimeck, M. A. Eriksson, M. Friesen, S. N. Coppersmith, P. von Allmen, F. Oyafuso, and S. Lee, Appl. Phys. Lett. **84**, 115 (2004).
[6] T. B. Boykin, G. Klimeck, M. Friesen, S. N. Coppersmith, P. von Allmen, F. Oyafuso, and S. Lee, Phys. Rev. B **70**, 165325 (2004).
[7] Y. Fu, M. Willander, E. L. Ivchenko, and A. A. Kiselev, Phys. Rev. B **47**, 13498 (1993).
[8] E. L. Ivchenko, A. A. Kiselev, Y. Fu, and M. Willander, Phys. Rev. B **50**, 7747 (1994).
[9] G. Klimeck, R. C. Bowen, T. B. Boykin, C. Salazar-Lazaro, T. A. Cwik, and A. Stoica, Superlattices Microstruct. **27**, 77 (2000).
[10] T. B. Boykin, G. Klimeck, R. C. Bowen, and R. Lake, Phys. Rev. B **56**, 4102 (1997).
[11] T. B. Boykin, G. Klimeck, and F. Oyafuso, Phys. Rev. B **69**, 115201 (2005).
[12] P. V. Santos, M. Willatzen, M. Cardona, and A. Cantarero, Phys. Rev. B **51**, 5121 (1995).
[13] L. Vervoort, R. Ferreira, and P. Voisin, Phys. Rev. B **56**, R12744 (1997).
[14] E. L. Ivchenko and M. O. Nestoklon, Phys. Rev. B **70**, 235332 (2004).
[15] P. Vogl, H. P. Hjalmarson, and J. D. Dow, J. Phys. Chem. Solids **44**, 365 (1983).
[16] M. M. Rieger and P. Vogl, Phys. Rev. B **48**, 14276 (1993).
[17] F. Schäffler, Semicond. Sci. Technol. **12**, 1515 (1997).
[18] M. M. Glazov, Phys. Rev. B **70**, 195314 (2004).
[19] E. L. Ivchenko, *Optical Spectroscopy of Semiconductor Nanostructures* (Alpha Sci. International Ltd., Harrow, UK, 2005).